Missouri University of Science and Technology

Scholars' Mine

International Conferences on Recent Advances in Geotechnical Earthquake Engineering and Soil Dynamics

1991 - Second International Conference on Recent Advances in Geotechnical Earthquake Engineering & Soil Dynamics

12 Mar 1991, 10:30 am - 12:00 pm

# Cyclic Undrained Behavior of an Undisturbed Gravel for Aseismic Design of a Bridge Foundation

Fumio Tatsuoka
*University of Tokyo, Japan*

Shin-Ichi Yamada
*Kisojiban Consultants, Co., Ltd., Japan*

Katsuhiko Yamada
*Honshu-Shiko Bridge Authority, Japan*

Masahiko Yasuda
*Honshu-Shiko Bridge Authority, Japan*

Susumu Manabe
*Japan Engineering Consultants, Co., Ltd., Japan*

Follow this and additional works at: https://scholarsmine.mst.edu/icrageesd

 Part of the Geotechnical Engineering Commons

## Recommended Citation

Tatsuoka, Fumio; Yamada, Shin-Ichi; Yamada, Katsuhiko; Yasuda, Masahiko; and Manabe, Susumu, "Cyclic Undrained Behavior of an Undisturbed Gravel for Aseismic Design of a Bridge Foundation" (1991). *International Conferences on Recent Advances in Geotechnical Earthquake Engineering and Soil Dynamics*. 10.
https://scholarsmine.mst.edu/icrageesd/02icrageesd/session01/10

This work is licensed under a Creative Commons Attribution-Noncommercial-No Derivative Works 4.0 License.

This Article - Conference proceedings is brought to you for free and open access by Scholars' Mine. It has been accepted for inclusion in International Conferences on Recent Advances in Geotechnical Earthquake Engineering and Soil Dynamics by an authorized administrator of Scholars' Mine. This work is protected by U. S. Copyright Law. Unauthorized use including reproduction for redistribution requires the permission of the copyright holder. For more information, please contact scholarsmine@mst.edu.

Proceedings: Second International Conference on Recent Advances in Geotechnical Earthquake Engineering and Soil Dynamics, March 11-15, 1991, St. Louis, Missouri, Paper No. 1.50

# Cyclic Undrained Behavior of an Undisturbed Gravel for Aseismic Design of a Bridge Foundation

**Fumio Tatsuoka**
Associate Professor, Institute Industrial Science, University of Tokyo, Roppongi, Minato-ku, Tokyo, Japan

**Shin-Ichi Yamada**
Kisojiban Consultants, Co., Ltd.

**Susumu Manabe**
Japan Engineering Consultants, Co., Ltd.

**Katsuhiko Yamada, Masahiko Yasuda**
Honshu-Shiko Bridge Authority

SYNOPSIS: For the aseismic design of a pier foundation constructed on a lightly cemented dense gravel deposit of a 3,910m-long suspension bridge, cyclic and monotonic undrained triaxial tests were performed on undisturbed specimens with a diameter of 30cm taken from the deposit under a sea depth of about 55m. Using the results of the cyclic undrained triaxial tests together with irregular cyclic stresses evaluated for the design earthquake motion by a dynamic FEM analysis, maximum strains in the gravel deposit were obtained by the cumulative damage concept. The strain values thus estimated indicated a sufficiently high degree of seismic stability of the foundation. Further, for the same initial mean principal stress, the strength for monotonic undrained triaxial compression of isotropically consolidated specimens was found not greater than the strength against irregular cyclic undrained loading of the specimens anisotropically consolidated as in the field. This means that the former strength can be used as an approximated value of the latter.

## INTRODUCTION

As a part of one of the three bridge routes connecting Main Island and Shikoku Island, a 3,910m-long suspension bridge Akashi Kaikyo Oh-Hashi is now under construction over a Akashi channel with a largest sea depth of about 110m (Figs. 1 and 2). The central span with a length of 1,990m will become longest in the world when constructed. Foundation 3P is founded on a stable sedimentary soft rock (Kobe Group) of Early Neogene Period of Tertiary Era, underlain by a granite bed rock (Fig. 3). Unlike the case of 3P, the seismic stability of Foundation 2P (Fig. 4) had been one of the major concerns in the design of this bridge, because 2P was to be placed on a weakly cemented gravel deposit (Akashi Group) having a largest thickness of about 50m. This deposit consists of round-shaped gravel particles and fine soils as the matrix filling the void of gravel, probably ancient river beds formed by mud flows of several million years ago in Late Neogene Period to Early Pleistocene Period. When studying the feasibility of the bridge, it was recognized that the strength and deformation properties of the gravel deposit obtained from field investigations involving bore hole lateral loading tests was not sufficient to determine confidently the dimensions and the depth of Foundation 2P. Further, the experience of the aseismic design of such a huge foundation on a gravel deposit as 2P was lacking. In view of the above, despite its very high cost, a large number of undisturbed samples were taken from the gravel deposit at the site of Foundation 2P.

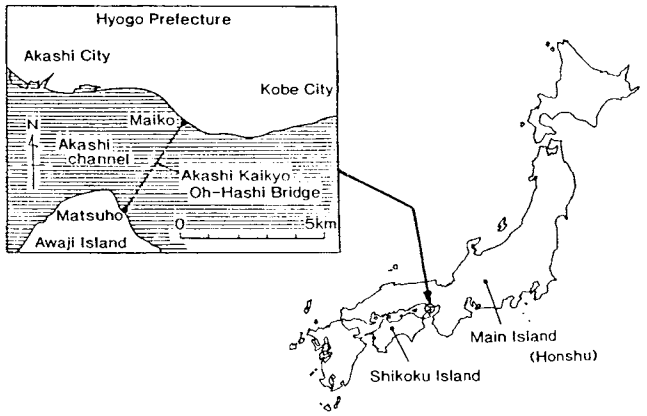


Fig. 1 Location of Akashi Kaikyo Oh-Hashi Bridge

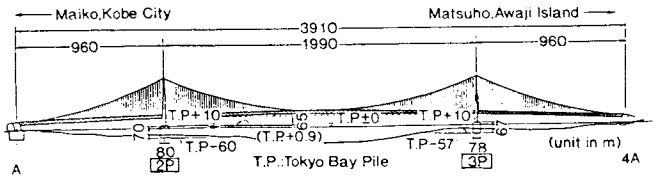


Fig. 2 Akashi Kaikyo Oh-Hashi Bridge

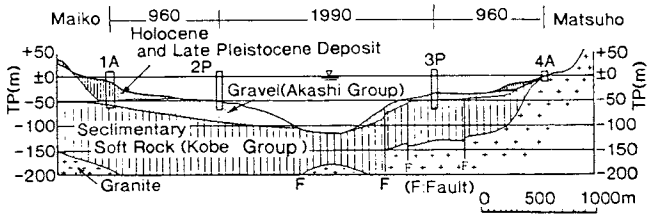


Fig. 3 Topographical and geological conditions

## TWO STAGES IN THE DESIGN OF FOUNDATION 2P

The first stage design was based on a simplified method using the results of triaxial compression tests and stability analyses by the pseudo-static limit equilibrium method within the framework of the conventional design methodology widely used in Japan. Yet, the method used was much more sophisticated than the ones currently used for the design of most bridges. In the second stage, a more sophisticated method was used for both the laboratory tests and the stability analyses taking into account the effects of earthquake on the load and the strength of soils in a more straightforward way. Yet, in order to balance against the limited amount of the data of the gravel deposit and uncertainties of the design earthquake motion, used was a method still simplified than the most sophisticated ones developed so far. It was attempted, therefore, that any simplification leads to a conservative or balanced result.

All the static and dynamic analyses of the foundation-ground system were performed under plane strain conditions in the transverse direction of the bridge, because in this direction, the effect of wind load is most critical under static conditions and the allowable displacement of the footing is minimum under seismic loading conditions.

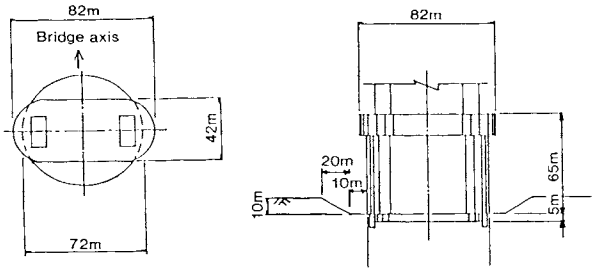


Fig. 4 Pier Foundation 2P (total weight= 653,472tons)

Stage I : Design by a conventional method

**(Step a)** The undisturbed samples with a diameter of 30cm were taken by offshore core-boring sampling from layers to a depth of about 40m below the sea bottom at a depth of about 55 m, using the largest offshore platform available in Japan. For this purpose, a large-diameter triple-tube sampling method was developed (Yamagata et al., 1987).

**(Step b)** About fifty drained and undrained monotonic triaxial compression tests were performed on isotropically consolidated specimens (Test Series 1), see Fig. 5. The relationship between the shear strength $\tau_f$ and the normal stress $\sigma_n'$ on the failure plane for the drained tests was determined from the envelop of the Mohr's circles shown in Fig. 5a. For the undrained tests, however, the $\tau_f$ value was not obtained from the envelop of the Mohr's circles with $\sigma_3 = \sigma_c'$ (the isotropic confining pressure at consolidation) (Fig. 5b)> This value was obtained from the shear stress corresponding to the effective mean principal stress $\sigma_m' = (\sigma_1' + 2\sigma_3')/3$ on the Mohr's circle of stress at the moment of the maximum deviator stress (Fig. 5c), which was assumed equal to the effective normal stress $\sigma_n'$ on the failure plane. In the same way, the initial normal stress $\sigma_{nc}'$ on the failure plane was assumed equal to the effective mean principal stress at consolidation $\sigma_{mc}'$, which was equal to the isotropic confining pressure $\sigma_c'$ for Series 1. Bothe the $\tau_f$ and $\sigma_n'$ relation for drained conditions and the $\tau_f$ and $\sigma_{nc}'$ relation (the failure line f-f in Fig. 5c) for undrained conditions used for the design are summarized in Fig. 6. These relations were determined by reducing to some extent the measured shear strength values in order to take into account the possible effects of the strength anisotropy and the progressive failure in the ground.

**(Step c)** The bearing capacity of Footing 2P under the design seismic condition was evaluated by the pseudo-static limit equilibrium method (Yamada, 1988). The effect of earthquake on the load was taken into account only in the footing load which was obtained from the earthquake response analysis of the bridge-foundation system. In the conventional aseismic design method currently used for smaller-scale bridges, the drained shear strength is used. In this case, under the most critical seismic loading condition, when the normal stress along the failure plane increases from the initial value $\sigma_{nc}'$ to $\sigma_{nc}' + \Delta\sigma_n'$, the drained strength $\tau_2$ is used (Fig. 6). For the design of Foundation 2P, however, the undrained shear strength $\tau_1$ corresponding to the initial stress $\sigma_{nc}'$ was used considering that $\sigma_n'$ will not increase with the increase in the total normal stress under seismic conditions. This was based on the following two considerations: (1) Due to a low permeability of the gravel deposit by the presence of fines soil matrix, the undrained conditions will prevail under seismic conditions. (2) The use of the undrained strength smaller than the the drained strength is conservative (see Fig. 6).

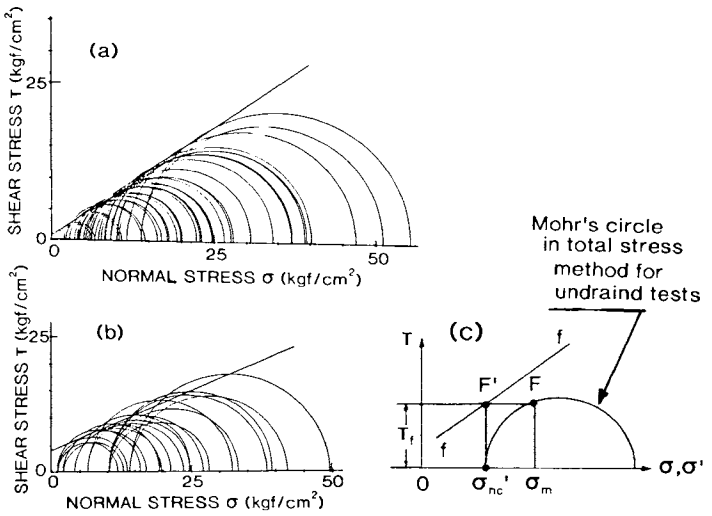


Fig. 5 Mohr's circles of stress at failure (isotropic consolidattion, $\sigma_3 = \sigma_c'$); (a) drained and (b) undrained tests (Test Series 1), and (c) the definitions of $\tau_f$ and $\sigma_n'$ for undrained tests

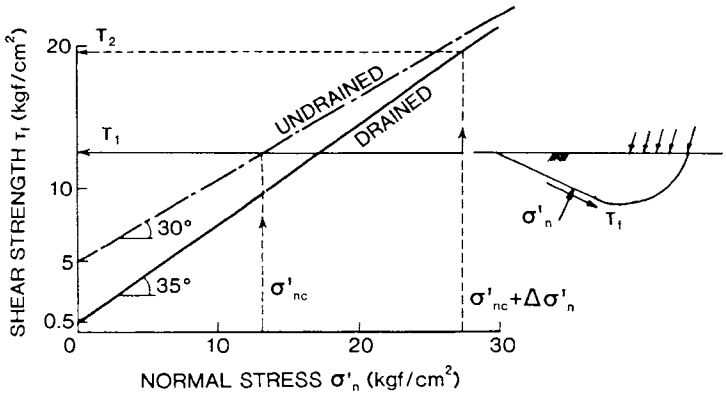


Fig. 6 Design strength used for pseudo-static stability analysis by the limit equilibrium method

Stage II : Confirmation of the the result of Stage I by a more sophisticated method

**(Step d)** The effects on the strength of both anisotropic initial stress conditions in the field and cyclic undrained loading during earthquakes were not taken into account in the design at Stage I. In order to evaluate these effects, a series of cyclic and monotonic undrained triaxial tests were performed on undisturbed specimens (Series 2).

**(Step e)** A FEM earthquake response analysis of the bridge-ground system was performed in order to obtain the time histories of random cyclic stresses within the ground.

**(Step f)** Maximum strain values which may develop in the gravel deposit supporting Foundation 2P during the design earthquake motion were estimated by means of the cumulative damage concept using the results of Steps d and e.

**(Step g)** Using the stiffness values of soil deteriorated due to cyclic undrained loading estimated by using the result of Step f, the maximum displacement of the foundation under the design seismic condition was estimated by a pseudo-static FEM analysis. Then, this was compared with its allowable design limit.

Herein reported is a part of the result of the investigation of Stage Ⅱ. The remaining part of the result will be reported elsewhere the future by the authors.

## TRIAXIAL SPECIMENS AND TESTING METHODS FOR TEST SERIES 2

At the site of sampling, each sample was trimmed to a length of about 60cm and the lateral surface and both ends were covered with 2mm-thick a rubber membrane and disks, respectively. The sample was confined in a steel mold to be transported to the laboratory. Although the density and grain size distribution characteristics were not very uniform among the samples as shown in Fig. 7 and Table 1, a particular variation in the test results was not observed.

Although it was not possible to evaluate exactly the effect of sampling disturbance, this effect was considered small because of a degree of natural cementation as reflected in some cohesion obtained by the drained triaxial compression tests (Fig. 5a). In addition, since the samples were very dense with a void ratio less than 0.5 (Table 1), the overall effect was considered to be a reduction in strength, the use of the strength as measured leading to a conservative result. Furthermore, it was considered unnecessary to take into account the membrane penetration effect on the results of undrained triaxial tests, because the lateral surface of sample was found smooth. Namely, the large particles at the lateral surface of sample had been cut according to the sample diameter by the core boring procedure and the void between gravel particles was filled with finer soils (Fig. 8).

Two monotonic loading triaxial compression tests (TC) and sixteen cyclic undrained triaxial tests (CTX) using uniform sine-wave cyclic stresses were performed at Institute of Industrial Science, University of Tokyo. Five specimens denoted as CTX-TC were loaded in monotonic triaxial compression following cyclic undrained loading without allowing drainage in between. Table 1 shows the test results of the specimens consolidated at a stress ratio $\sigma_{1c}'/\sigma_{3c}'=3$.

Being confined at a cell pressure of 0.3kgf/cm², the dimensions of specimens were measured and the specimens were made fully saturated by the dry setting method (ASTM D4767). Namely, a partial vacuum of 0.95kgf/cm² was applied to the inside of specimen, while a partial vacuum of 0.65kgf/cm² was applied to the inside of the cell (i.e., the outside of the specimen). Then, with keeping the effective stress at 0.3 kgf/cm², a back pressure of 2.0kgf/cm² or more was applied. The measured pore pressure coefficients B were 0.96 or more (Table 1). The method of saturation by percolating $CO_2$ gas and de-aired water through a specimen was found ineffective due to its very low permeability.

The pressure levels and stress ratios used for consolidating the specimens were (1) the stress ratio $\sigma_{1c}'/\sigma_{3c}'=2$, 3 and 4 for the mean principal stress $\sigma_{mc}'=(\sigma_{1c}'+2\cdot\sigma_{3c}')/3=6.67$kgf/cm² and (2) $\sigma_{1c}'/\sigma_{3c}'=1$ for $\sigma_{mc}'=4.0$/cm² which were determined from the result of a static FEM analysis (Fig. 9). In Fig. 9, some white zones near the ground surface means fictitious tensile stresses. These were obtained because the same Young's modulus was used in all the elements of the Akashi gravel deposit and the overlying layer. The value of $\sigma_{mc}'$ was estimated by assuming $\sigma_{zc}'=\sigma_{3c}'$ in the ground. The results show that $\sigma_{mc}'$ is around 6 - 8kgf/cm² in the layers beneath the footing and around 4kgf/cm² in the zones adjacent to the footing. The value of $\sigma_{1c}'/\sigma_{3c}'$ is around 3 in the layers beneath the footing, but smaller in the zones adjacent to the footing. In this paper, only the test results for $\sigma_{1c}'/\sigma_{3c}'=3$ and $\sigma_{mc}'=6.67$kgf/cm² are reported.

For anisotropic consolidation, a specimen was first isotropically consolidated to the final value of $\sigma_{3c}'$ and then only the axial stress was increased under drained conditions, by assuming that the design earthquake may attack the bridge after the excess pore water pressure developed by the construction of the foundation has dissipated. For cyclic loading, uniform cyclic stresses of 0.1Hz were used, while for monotonic loading, the specimen was compressed at a constant axial strain rate of 0.1%/minute.

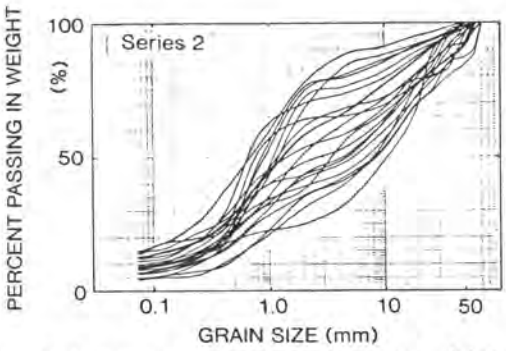


Fig. 7 Grain size distribution curves of triaxial specimens (Series 2)

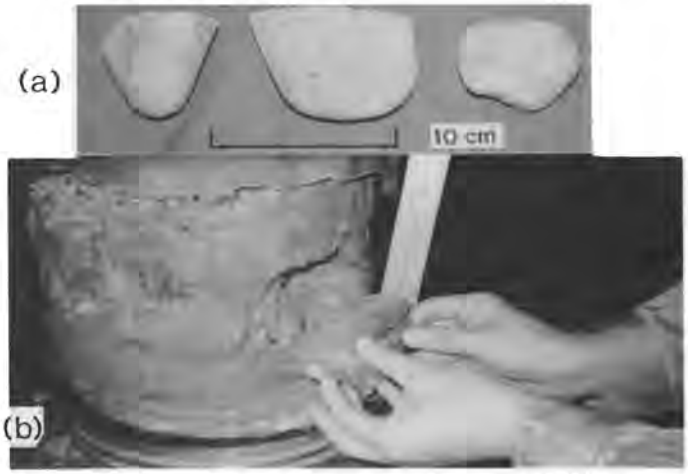


Fig. 8 (a) Gravels cut during core boring and (b) view of a specimen after test (A piece of gravel being removed from the specimen)

Due to the limited depth of sampling, most of the triaxial specimens were used to represent in-situ layers deeper than those from which they were taken. For the case of $\sigma_{1c}'/\sigma_{3c}'=3$, the ratio in depth is about three (see the depth ratios shown in Table 1). Therefore, even if the soils in the field are overconsolidated, it is unlikely that the field cyclic undrained strength values were over-estimated by testing at OCR ratios larger than those in the field. Further, the effect of this difference would be small for the layers beneath the foundation, because by the load of the footing, they will be consolidated to normally consolidated conditions or near them.

In monotonic triaxial tests, the principal stress directions do not rotate, and in cyclic triaxial tests, they may rotate by 90 degrees abruptly with no shear stress. Therefore, since they rotate continuously in the field, in general its effect should be taken into account when using the triaxial test results. Fig. 11 shows the maximum rotation angle $\theta_{d\text{-}max}$ of the principal stress direction from the static condition caused by the design earthquake motion. The double amplitude angle of the rotation is the double of $\theta_{d\text{-}max}$ at the largest, but not larger than 90 degrees. It may be seen that $\theta_{d\text{-}max}$ decreases as $\sigma_{1c}'/\sigma_{3c}'$ increases. In most of the elements beneath the foundation (e.g., Elements E, G, I and K), $\theta_{d\text{-}max}$ are less than about 10 degrees. It was considered that when the rotation is small

Table 1 Test conditions and results ( $\sigma_{1c}'/\sigma_{3c}'$=3)

| Test type | TC | CTX | | | | | |
|---|---|---|---|---|---|---|---|
| Specimen No. | 1-6 | 5-10 | 6-8 | 6-11-1 | 5-15 | 6-9 | 6-12 |
| Sampling depth[1] (m) | 3.6 | 9.4 | 10.5 | 13.6 | 12.0 | 11.5 | 10.9 |
| Depth ratio[2] | 0.11 | 0.29 | 0.32 | 0.42 | 0.39 | 0.35 | 0.33 |
| $\rho_t$ (g/cm³) | 2.158 | 2.043 | 2.151 | 2.126 | 2.120 | 2.121 | 2.184 |
| $\rho_d$ (g/cm³) | 1.862 | 1.837 | 1.858 | 1.907 | 1.834 | 1.887 | 1.916 |
| Intial void ratio e | 0.434 | 0.435 | 0.426 | 0.365 | 0.446 | 0.386 | 0.392 |
| Gravel content (%) | 57 | 68 | 59 | 23 | 36 | 64 | 38 |
| Sand content (%) | 38 | 24 | 40 | 61 | 55 | 29 | 53 |
| Fines content (%) | 6 | 8 | 1 | 16 | 9 | 7 | 9 |
| Axial strain (%) | 0.77 | 0.61 | 0.81 | 0.82 | 0.62 | 0.88 | 0.92 |
| Volumetric strain(%) (during isotropic consolidation) | 2.22 | 2.02 | 3.57 | 2.40 | 2.12 | 3.27 | 2.92 |
| B value | 0.96 | 0.98 | 0.98 | 0.97 | 0.96 | 0.98 | 0.98 |
| $\sigma_d/2\cdot\sigma_{mc}'$ | (22.347)[3] | 0.204 | 0.329 | 0.513 | 0.593 | 0.293 | 0.458 |
| $N_c$ at $\varepsilon_a'$=0.2% | - | 3.6 | 0.14 | - | - | 0.17 | - |
| $N_c$ at $\varepsilon_a'$=0.5% | - | 33 | 0.33 | 0.15 | 0.1 | 1.65 | 0.12 |
| $N_c$ at $\varepsilon_a'$= 1% | - | - | 2.5 | 0.44 | 0.2 | 5.6 | 0.25 |
| $N_c$ at $\varepsilon_a'$= 2% | - | - | 10.0 | 3.5 | 1.25 | 36 | 2.25 |
| $N_c$ at $\varepsilon_a'$= 5% | - | - | 96 | 16.3 | 8.0 | - | 24 |
| $N_c$ at $\varepsilon_a'$=10% | - | - | - | 64 | 25 | - | 95 |
| $\varepsilon_a'$(%) at $N_c$= 500 | - | 1.0 | 7.8 | - | - | 4.1 | - |
| Max. $\Delta u$ (kgf/cm²) | -2.281 | 1.496 | 1.936 | 2.222 | 2.962 | 1.548 | 2.305 |

1) Depth from the sea bottom. 2) (the depth of sampling)/(the depth of the layer modeled in the test= 32.5m). 3) The maximum deviator stress; $(\sigma_1-\sigma_3)_{max}$

as the above, its possible effect on the strength and deformation properties of soils be negligible and the simulation by the cyclic triaxial tests without the rotation of the principal stress direction would be relevant. On the other hand, when $\sigma_{1c}'/\sigma_{3c}'$ decreases from 2.0, the rotation increases largely. It was considered that the behavior in this case can be simulated by the cyclic triaxial tests with a rotation of 90 degrees in the principal stress directions. It was found afterwards from the results of the cyclic undrained tests that the relationship between the maximum axial strain in each loading cycle and the amplitude of cyclic stress was rather independent of $\sigma_{1c}'/\sigma_{3c}'$ between 1.0 and 4.0, thus independent of whether the principal stresses rotated or not in the tests. Based on the above, the simulation of the field seismic conditions by the cyclic triaxial testing was considered relevant for the purpose of this investigation.

For all the specimens, the direction of $\sigma_1'$ during consolidation was in the in-situ vertical direction. Therefore, if the effect of the possibly anisotropic fabric of the specimens on the test results is significant, this should be taken into account. However, this effect was considered small by the following reasons: (1) In the cyclic undrained tests on isotropically consolidated specimens with symmetric cyclic stresses in triaxial compression and extension, the axial strains developed were rather symmetric. Further, the strains developed during isotropic consolidation were rather isotropic (see Table 1). These results suggested that the specimens were rather isotropic. (2) In the gravel layers supporting the foundation, of which the strength values were most concerned, the angle $\theta$ of the direction of $\sigma_1'$ relative to the vertical under the static stress condition was very small (see Fig. 9c).

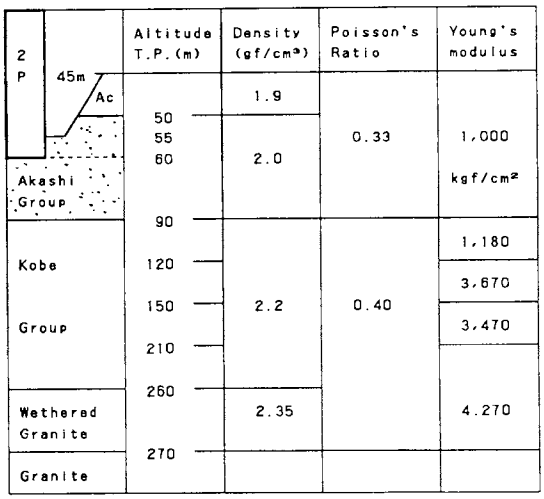


Ac: Late Pleistocene and Holocene deposit

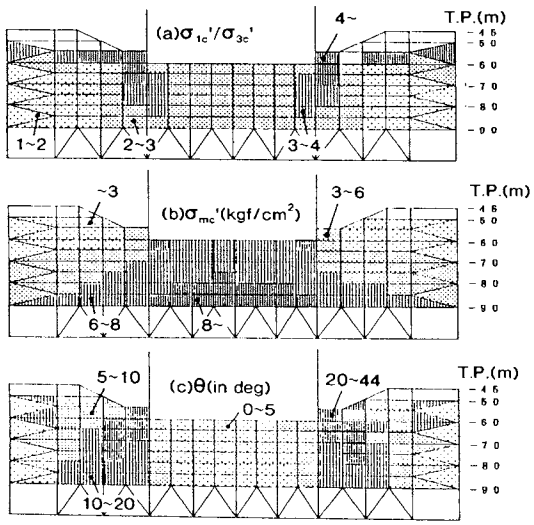


Fig. 9 Model and results of static FEM analysis; $\theta$ = the angle of $\sigma_1$ relative to vertical in degree

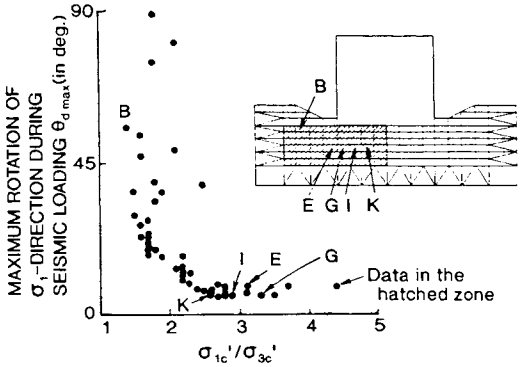


Fig. 10 $\theta_{d\text{-}max}$ (Fig. 16b) and $\sigma_{1c}'/\sigma_{3c}'$ (Fig. 9) relations obtained by FEM analyses

In the triaxial tests, $\sigma_2'$ equals either $\sigma_1'$ or $\sigma_3'$, whereas it is between them in the field. It was considered conservative to ignore the effect of this difference on both the monotonic and cyclic undrained strengths, because it is known that the others being the same, the monotonic strength is smaller in triaxial compression than in plane strain and the cyclic undrained strength is smaller in triaxial compression and extension than in plane strain.

## TEST RESULTS OF CYCLIC TESTS for $\sigma_{1c}'/\sigma_{3c}'=3$

Figs. 11, 12a and 12b show some of the test results of CTX. Fig. 12c shows the stress paths typical of the monotonic undrained triaxial compression tests on isotropically consolidated specimens of Series 1. As may be seen from Figs. 11 and 12, the specimen subjected to cyclic undrained loading behaved like a very densely packed sand in that the rate of the increase in the axial strain with cyclic loading never increased even after the effective stress path was approaching the failure envelope. Further, due to the property of cyclic mobility, the specimens could sustain cyclic stresses having a maximum deviator stress close to the drained strength without exhibiting large strains.

The proper definition of the cyclic undrained strength of saturated soils has been a controversial topic. The steady state strength proposed by Casagrande and his colleagues (e.g., Poulos et al., 1985) was not employed, because when following this definition, the development of strain during an earthquake motion cannot be traced. Besides, the use of such a strength defined for large strains is not relevant for the stability analysis of this bridge which is sensitive to even small displacement of the foundations. On the other hand, Seed (e.g., Seed, 1987) recommended the use of so-called initial liquefaction strength as obtained from CTX tests on isotropically consolidated specimens for the purpose of the liquefaction analysis of level ground. This definition was not employed either, because in this study, even in the CTX tests on the isotropically consolidated specimens, the axial strain did not started to increase suddenly even after the moment of initial liquefaction. Further, in the CTX tests on anisotropically consolidated specimens, axial strain increases without reaching the condition of initial liquefaction (see Figs. 11 and 12). Andersen et al. (1988) defined the strength for the mean strain value ( $\varepsilon_1^+ + \varepsilon_1^-)/2$ to evaluate the residual deformation of the ground and also for the strain amplitude ( $\varepsilon_1^+ - \varepsilon_1^-$) to evaluate the cyclic deformation of the ground (see Fig. 13). In this study, the strength was defined as the amplitude of cyclic stress for a certain maximum axial strain $\varepsilon_1^+$ in a certain loading cycle by the following reasons: (1) The allowable maximum displacement of the foundation is specified under design seismic conditions based on the allowable maximum deformation of the superstructure of the bridge. In order to evaluate this value, the definition based on $\varepsilon_1^+$ is most relevant. (2) This definition can be used equally for any value of $\sigma_{1c}'/\sigma_{3c}'$. Fig. 14 shows the test results summarized based on this definition.

## EARTHQUAKE RESPONSE ANALYSIS

Using equivalent shear muduli and damping values as a function of cyclic shear strain $\gamma$, an equivalent linear FEM earthquake response analysis was performed in frequency domain (Fig. 15). The earthquake input motion (Fig. 15b) was given at the surface of unweathered granite rock. The initial shear moduli $G_{max}$ at $\gamma = 10^{-6}$ were obtained from the field shear wave velocity $V_s$. The properties shown in Fig. 16c were obtained from another series of cyclic triaxial tests on undisturbed specimens with a diameter of 30cm and 5cm for Akashi and Kobe Groups, respectively.

A part of the results are shown in Fig. 16. Due to the rocking behavior of the footing, cyclic stresses induced were relatively large in the zones beneath the edge of footing (e.g., Elements E and G), but small along the central line of the footing (e.g., Element K). In the zones beneath the footing (e.g., Elements G, I and K), the largest rotation angle in double amplitude of the principal stress direction is not greater than 20 degrees. Therefore, the effect of the rotation of the principal stress direction would be very small. However, this is not be small in the zones adjacent to the footing (e.g., Element B).

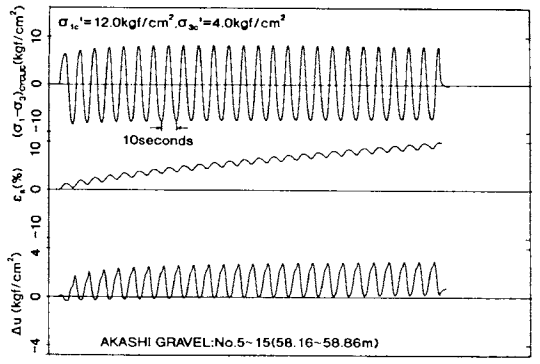


Fig. 11 Typical time histories of cyclic deviator stress, axial strain and excess pore water pressure

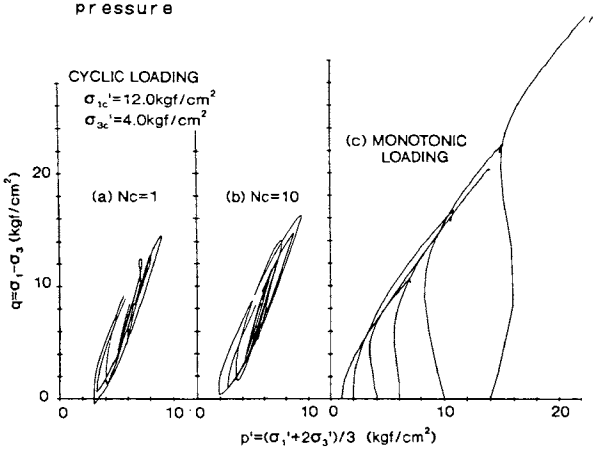


Fig. 12 Stress paths (a) and (b) cyclic tests ( $\sigma_{1c}'/\sigma_{3c}'=3$)and (c) monotonic undrained triaxial compression tests (isotropical consolidation)

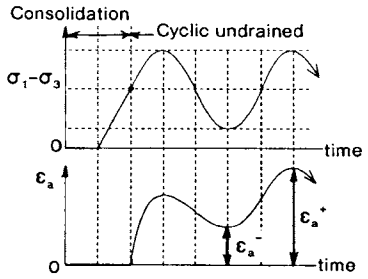


Fig. 13 Definitions of stresses and strains

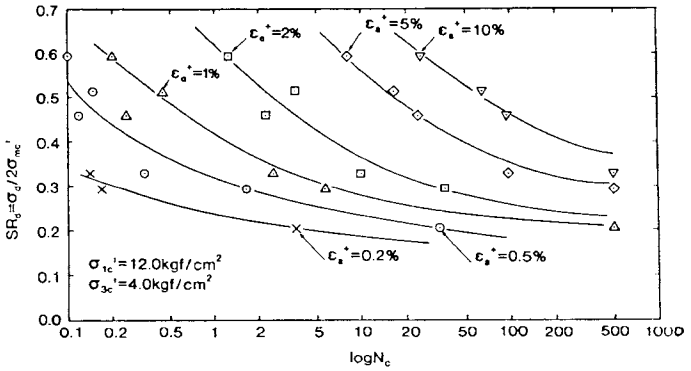


Fig. 14 $S_d = \sigma_d/(2\sigma_{mc}') \sim N_c$ relations for $\sigma_{1c}'/\sigma_{3c}'=3$, $\sigma_d=(\sigma_1'-\sigma_3')_d$

## STRAINS BY IRREGULAR CYCLIC STRESSES ESTIMATED BY CUMULATIVE DAMAGE CONCEPT

The maximum strain values in the gravel deposit under the design seismic condition were estimated by the cumulative damage concept (CDC) (Donovan, 1971), using half pulses of cyclic stresses (Tatsuoka et al., 1986) in the following way:

(1) For each element, a series of half pulse SR(n) is defined from the time history of $\sigma_1' - \sigma_3'$ obtained for the design earthquake motion in such a way as that the nth half pulse $SR(n) = (\sigma_1' - \sigma_3')_{cycle}/(2\sigma_{mc}')$. $(\sigma_1' - \sigma_3')_{cycle}$ is the amplitude of the nth half pulse between two successive zero-crossing points (Fig. 17). The largest SR(n) is defined as SR(1). Then, the accumulative curves of half pulse are obtained (Fig. 18). Only such accumulative curves are needed for the CDC analysis, because the result is independent of the sequence of pulse.

(2) For each element, strength curves defined for different strain values are prepared as shown in Fig. 19. These shown in Fig. 19 were made from those shown in Fig. 14.

(3) For a certain strain value $\varepsilon_1^+$ selected, the total damage D for such a given accumulative curve of half pulse as shown in Fig. 18 is computed as $D = \Sigma\, 1/\{2 \cdot N_c(n)\}$. $N_c(n)$ is the number of cycle which corresponds to the value of $SR_d$ equal to SR(n) for such a strength curve for the given value of $\varepsilon_1^+$ as shown in Fig. 19.

(4) The step (3) is repeated by multiplying all the half pulses by a constant, but fixed at each calculation, factor $\alpha$ until the value of D becomes 1.0. The value of $\alpha \cdot SR(1)$ for D= 1.0 is defined as $SR(1)_{D=1}$ for the given value of $\varepsilon_1^+$.

(5) The steps (3) and (4) are repeated by changing the value of $\varepsilon_1^+$ to obtain the $SR(1)_{D=1} \sim \varepsilon_1^+$ relation as shown in Fig. 20 for each element. The difference seen in the results is due to the different randomness in cyclic stresses; i.e., the different patterns of accumulative curve of half pulse.

That value of $\varepsilon_1^+$ which corresponds to $SR(1)_{D=1} = SR(1)$ (i.e., $\alpha = 1.0$) is the largest strain expected for the given design earthquake motion. These values are very small for Elements E, G and I (Fig. 20).

Fig. 21 shows the distribution of $\varepsilon_1^+$ for the given design earthquake motion (i.e., for $\alpha = 1.0$). It may be seen that the strains in the layers supporting the footing are not greater than 0.2% and smaller in the zones closer to the central line of the footing. These results already show that the displacement of the footing during the design earthquake motion would be very small. However, Fig. 21 shows so-called strain potential, which does not satisfy the strain compatibility within the ground. A pseudo-static FEM analysis, which satisfies the strain compatibility, showed that the maximum horizontal relative displacement between the top and bottom of Foundation 2P under the design seismic condition is about 2.4cm, which was about 1/3.5 of the allowable limit. This result will be reported more in details elsewhere.

The method described above is a total stress method in which the stiffness values used in the earthquake response analysis do not match those obtained by using CDC. Namely, the former values are a function of the initial consolidation stress, thus, larger than the latter which has deteriorated due to the development of pore water pressure by undrained cyclic loading. Therefore, the first natural period of the foundation-ground system of about 0.8 second obtained by the earthquake response analysis is somehow underestimated. Since this natural period is larger than the predominant period of the input earthquake motion of about 0.2-0.3 seconds, the underestimated natural period leads to overestimated cyclic stresses. Therefore, in this case, the use of such a total stress method as above would be conservative.

(a)

| | | Altitude T.P.(m) | Density (gf/cm³) | Vs (m/s) | Poisson's Ratio | Initial Damping |
|---|---|---|---|---|---|---|
| 2P | | 55 | 2.0 | 700 | 0.43 | 0.013 |
| | Akashi Group | 60 | | 600 | | 0.024 |
| | | 75 | | 630 | | |
| | Kobe Group | 90 | 2.2 | 910 | 0.40 | 0.043 |
| | | 120 | | 790 | 0.43 | 0.051 |
| | | 150 | | 1,000 | 0.41 | 0.043 |
| | | 210 | | | | |
| | Wethered Granite | 260 | 2.35 | | | 0.046 |
| | Granite | 270 | 2.35 | 1,080 | 0.40 | 0.045 |

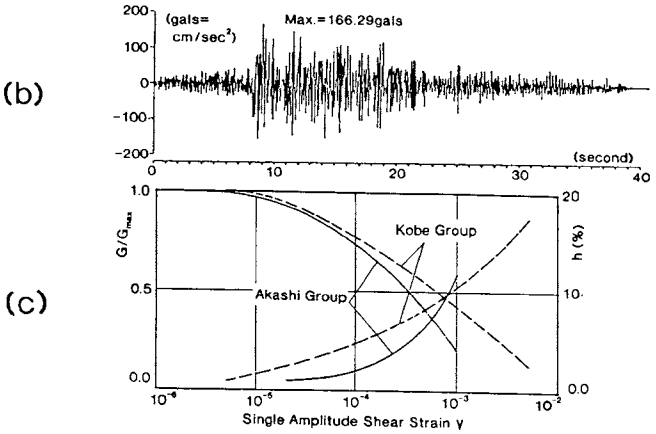


Fig. 15 (a) Model, (b) input time history of acceleration, and (c) strain-level dependency of stiffness and damping for dynamic FEM analysis

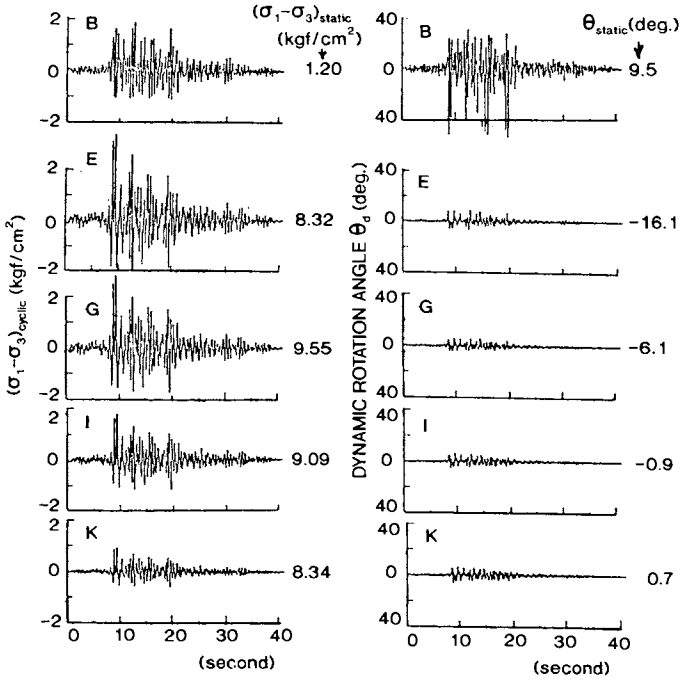


Fig. 16 Some typical time histories of (a) $\sigma_1' - \sigma_3'$ and (b) angle $\theta$ of the direction of $\sigma_1$ relative to the vertical by FEM analysis (see Fig. 10 for the locations of the elements)

## COMPARISON OF CYCLIC AND MONOTONIC LOADING BEHAVIORS

Fig. 22 compares the following three kinds of stress-strain relations in monotonic undrained triaxial compression:
(1) That of a specimen isotropically consolidated at $\sigma_{mc}'$= 6.67kgf/cm², obtained by interpolating those relations at $\sigma_{mc}'$= 4, 6 and 10 kgf/cm² of Series 1 from which the design strength was determined (see Fig. 6). In Fig. 22a, the point of zero-axial strain for this test was made located at the point A at which the axial strain was defined as zero for the following tests on anisotropically consolidated specimens. The stress value at an axial strain of 2%, Strength I,

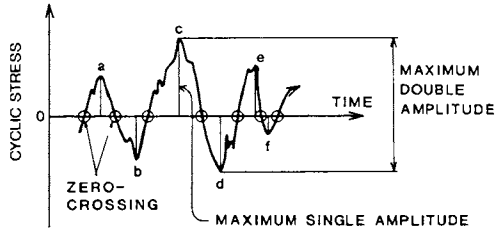


Fig. 17 Definition of zero-crossing point

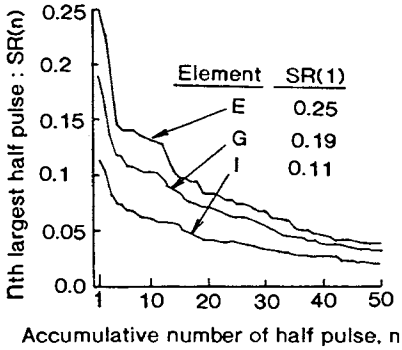


Fig. 18 Accumulative curves of half pulse from the largest pulse for the design earthquake motion for Elements E, G and I

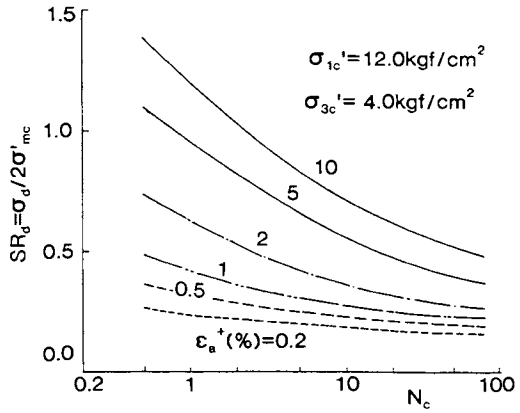


Fig. 19 Strength curves for Elements E, G and I used for CDC analysis (the portions for $SR_d$ > 0.6 were obtained by extrapolating the test results)

is plotted in Fig. 23a.
(2) That of a specimen anisotropically consolidated at $\sigma_{mc}'$= 6.67kgf/cm² and $\sigma_{1c}'/\sigma_{3c}'$= 3. The strength obtained from this test, Strength A, also is shown in Fig. 23a.
(3) Those of the three specimens having been subjected to cyclic undrained loading. They had been initially anisotropically consolidated at $\sigma_{mc}'$= 6.67kgf/cm² and $\sigma_{1c}'/\sigma_{3c}'$= 3. These specimens were selected for this kind of test because they did not exhibit excessive strains in cyclic undrained loading. These tests were performed to evaluate the post-earthquake undrained strength.

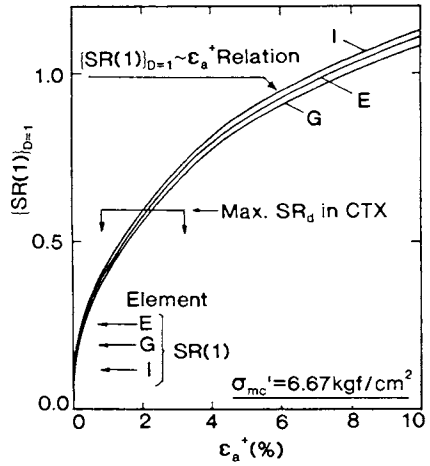


Fig. 20 $SR(1)_{D=1} \sim \varepsilon_1^+$ relations, Elements E, G and I

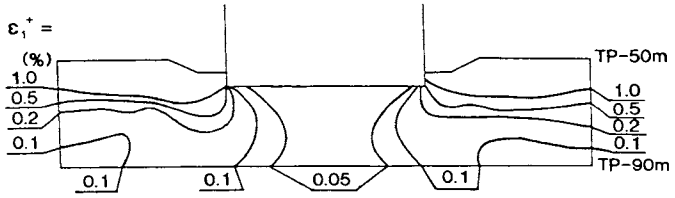


Fig. 21 Distribution of $\varepsilon_1^+$ for the design earthquake motion

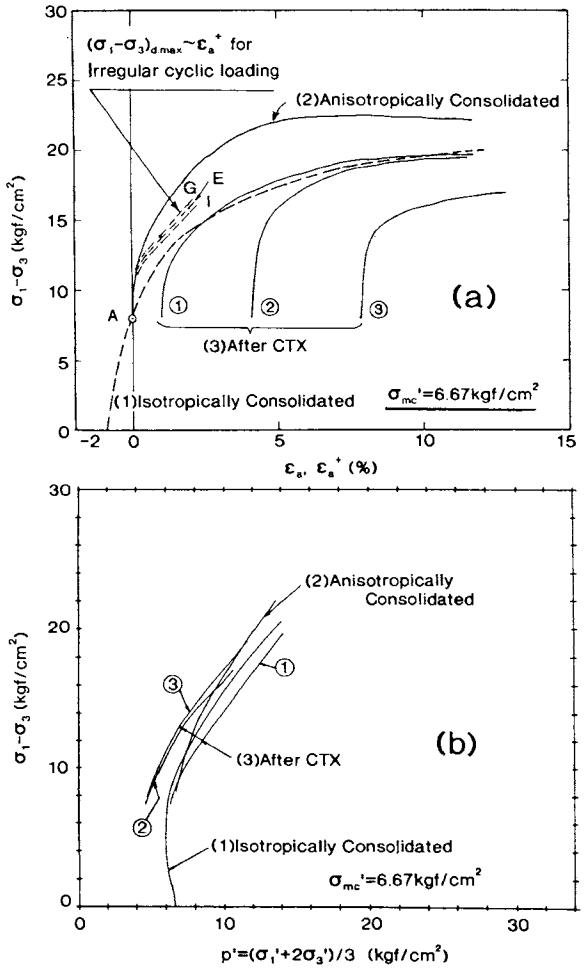


Fig. 22 (a) Stress-strain relations and (b) stress paths for monotonic and cyclic undrained loading

Also in Fig. 22a are shown the relationships between the maximum deviator stress ( $\sigma_1'-\sigma_3')_{d\text{-}max}$ and the value of $\varepsilon_1^+$ estimated for seismic loading conditions by using CDC. Here, ( $\sigma_1'-\sigma_3')_{d\text{-}max}$ is the deviator stress at consolidation (= $\sigma_{1c}'-\sigma_{3c}'$) plus the maximum cyclic deviator stress (= $\{SR(1)\}_{D=1}\cdot 2\cdot \sigma_{mc}'$) used to calculate $\varepsilon_1^+$. In Fig. 22, the relations are shown only for a range of the deviator stress below its largest value used in the CTX tests. In Fig. 23a, Strength C defined for $\varepsilon_1^+=2\%$ is also shown (the points E, G and I).

In Figs. 22 and 23, the relationships are compared for the same $\sigma_{mc}'$ (= 6.67kgf/cm²). This was to compare the behavior at the similar effective normal stress at consolidaton $\sigma_{nc}'$ on the failure plane, assuming that also for anisotropically consolidated specimens, $\sigma_{mc}'$ be equal to $\sigma_{nc}'$ (see Fig. 23b).

The following points may be seen from Figs. 22 and 23:
(1) For the specimens without a cyclic undrained loading history, the strength of the anisotropically consolidated one (Strength A) is larger than that of the isotropically consolidated one (Strength I). This was due probably to that the reduction in the effective mean principal stress during undrained shearing from $\sigma_1'/\sigma_3'=1.0$ to 3.0 by the tendency of volume decrease (i.e., negative dilatancy) observed in the isotropically consolidated specimen was not involved in the behavior of the anisotropically consolidated specimen. Therefore, when considering this factor alone, the use of Strength I for the in-situ anisotropic stress conditions leads to a conservative result.

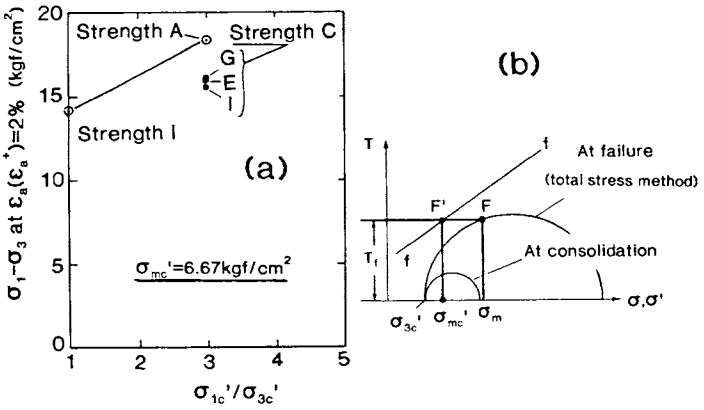


Fig. 23 (a) Strength defined for $\varepsilon_1$ ( $\varepsilon_1^+$)= 2% versus $\sigma_{1c}'/\sigma_{3c}'$ and (b) the definition of $\sigma_{mc}'$

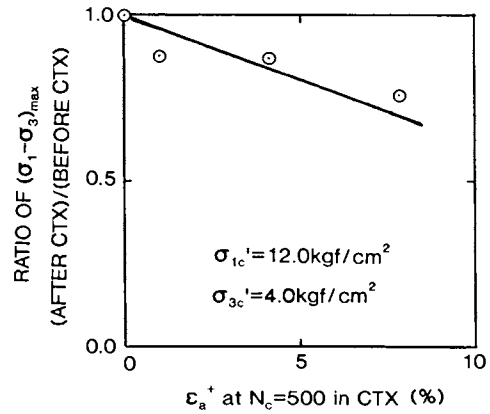


Fig. 24 Ratio of monotonic undrained strength in the cases with and without previous cyclic undrained loading versus the axial strain observed at $N_c$= 500 in cyclic undrained loading

(2) For the anisotropically consolidated specimens, the strength against irregular cyclic undrained loading (Strength C) is smaller than that against monotonic undrained loading (Strength A). This is due to the softening caused by cyclic undrained loading. Therefore, when considering this factor alone, the use of the monotonic loading strength (Strength A) for seismic loading conditions leads to a unconservative result. However, Strength C is larger than Strength I due to the combined effect of anisotropic consolidation and cyclic undrained loading. Therefore, the use of Strength I as an approximated design strength value for the field seismic conditions seems relevant.
(3) For the anisotropically consolidated specimens, the strength against monotonic undrained loading decreased only slightly by previous undrained cyclic loading (see also Fig. 24). Since the strain values which may occur during the design earthquake motion is very small (see Fig. 21), it can be considered that a catastrophic failure of the foundation, as may occur for the one on a loose saturated sand deposit, will never occur.

## CONCLUSIONS

The triaxial testing was the only possible laboratory testing method for evaluating the monotonic and cyclic undrained strengths of the undisturbed gravel samples with a diameter of 30cm, despite some limitation inherent to this testing method. The data obtained from this test program seems very useful also for other similar projects, because the available data set of gravel like this is very limited. The cyclic undrained strength of these samples was found larger than anticipated beforehand. Using the test results, the maximum strains during the design seismic condition in the lightly cemented gravel layers supporting the bridge foundation concerned were calculated by the cumulative damage concept. These strain values in the zones beneath the footing were found not greater than 0.2%. This means that the maximum displacement of the foundation expected under the design seismic condition will be well within the design limit. It was also found that the effect of both anisotropic consolidation and cyclic undrained loading should be taken into account for the proper evaluation of the 'dynamic' strength of soils under anisotropic stress conditions.

## ACKNOWLEDGEMENTS

The authors are very grateful to Mr. T. Yamashita of Kisojiban Consultants Co., Ltd., Mr. N. Hamori of Japan Engineering Consultants Co., Ltd. and Mr. T. Sato and Mis M. Torimitsu of Institute of Industrial Science, University of Tokyo for their cooperation provided to the research program.

## REFERENCES

Andersen, K. H., Kleven, A. and Heien, D., "Cyclic Soil Data for Design of Gravity Structures," Jour. Geotechnical Engrg, 114-5, 1988, 517-539.
Poulos, S. J., Castro, G. and France, J. W., "Liquefaction Evaluation Procedure," Jour. Geotechnical Engrg, 111-6, 1985, 772-792.
Seed, H. Bolton, "Design Problems in Soil Liquefaction," Jour. Geotechnical Engrg, 113-8, 1987, 827-845.
Tatsuoka, F., Maeda, S., Ochi, K. and Fujii, S., "Prediction of Cyclic Undrained Strength of Sand Subjected to Irregular Loading," Soils and Foundations, 26-2, 1986, 73-90
Yamada, M., "Geotechnical Investigation and Design of Pier Foundation for Akashi Kaikyo Oh-Hashi Bridge," Lecture Note for Seminar on Recent Issues of Geotechnical and Foundation Engineering, Japanese Society of SMFE, 1988, 137-146 (in Japanese).
Yamagata, M., Suzuki, M. and Fujiwara, T., "Soil Sampling in Akashi Kaikyo Channel," Chishitsu-to-Chosa, 1987, Vol.2, 32-37 (in Japanese)